Magnetic structure and ferroelectric polarization of $MnWO_4$ investigated by density functional calculations and classical spin analysis

Chuan Tian,[1] Changhoon Lee,[1] Hongjun Xiang,[2] Yuemei Zhang,[1] Christophe Payen,[3] Stéphane Jobic,[3] and Myung-Hwan Whangbo[1]

[1]*Department of Chemistry, North Carolina State University, Raleigh, North Carolina 27695-8204, USA*

[2]*National Renewable Energy Laboratory, Golden, Colorado 80401, USA*

[3]*Institut des Matériaux Jean Rouxel, Université de Nantes–CNRS, 2 rue de la Houssinière, BP 32229, 44322 Nantes, France*

(Received 5 June 2009; revised manuscript received 10 August 2009; published 22 September 2009)

The ordered magnetic states of $MnWO_4$ at low temperatures were examined by evaluating the spin exchange interactions between the Mn^{2+} ions of $MnWO_4$ on the basis of first principles density functional calculations and by performing classical spin analysis with the resulting spin exchange parameters. Our work shows that the spin exchange interactions are frustrated within each zigzag chain of Mn^{2+} ions along the *c* direction and between such chains of Mn^{2+} ions along the *a* direction. This explains the occurrence of a spiral-spin order along the *c* and *a* directions in the incommensurate magnetic state AF2, and that of a $\uparrow\uparrow\downarrow\downarrow$ spin order along the *c* and *a* directions in the commensurate magnetic state AF1. The ferroelectric polarization of $MnWO_4$ in the spiral-spin state AF2 was examined by performing Berry phase calculations for a model superstructure to find that the ferroelectric polarization occurs along the *b* direction, in agreement with experiment.

DOI: 10.1103/PhysRevB.80.104426 PACS number(s): 75.25.+z, 71.70.Gm, 71.70.Ej

I. INTRODUCTION

Manganese tungstate $MnWO_4$ is made up of MnO_6 octahedra with high-spin Mn^{2+} (d^5) ions and WO_6 octahedra with diamagnetic W^{6+} (d^0) ions.[1–3] The MnO_6 octahedra share their *cis* edges to form zigzag MnO_4 chains along the *c* direction [Fig. 1(a)]. Similarly, the WO_6 octahedra share their *cis* edges to form zigzag WO_4 chains along the *c* direction [Fig. 1(b)]. These MnO_4 and WO_4 chains share their octahedral corners to form the three-dimensional structure of $MnWO_4$ [Fig. 1(c)]. As a result, layers of Mn^{2+} ions parallel to the *bc* plane (hereafter, the //*bc* layers of Mn^{2+} ions) alternate with layers of W^{6+} ions parallel to the *bc*-plane along the *a* direction. The neutron diffraction study by Lautenschläger *et al.*[3] established that $MnWO_4$ undergoes three magnetic phase transitions below 14 K, namely, the paramagnetic to the AF3 state at T_N (13.5 K), the AF3 to the AF2 state at T_2 (12.3 K), and the AF2 to the AF1 state at T_1 (8.0 K). The magnetic structures of the AF3 and AF2 states are incommensurate with the propagation vector (−0.214, 0.5, 0.457), while that of the AF1 state is commensurate with the propagation vector (−0.25, 0.5, 0.5). Ehrenberg *et al.*[4] analyzed the spin wave dispersion curves of the magnetic state AF1 of $MnWO_4$, determined from inelastic neutron scattering measurements,[4] in terms of nine spin-exchange parameters (Fig. 2, Table I); the exchanges J_1 and J_2 in the zigzag chains of Mn^{2+} ions along the *c* direction (hereafter, the //*c* chains of Mn^{2+} ions), the exchanges J_3 and J_4 between adjacent //*c* chains of Mn^{2+} ions in each //*bc* layer of Mn^{2+} ions, and the exchanges J_5–J_9 between the adjacent //*bc* layers of Mn^{2+} ions along the *a* direction. So far, it has not been tested whether the values of J_1–J_9 extracted by Ehrenberg *et al.*[4] are consistent with other magnetic properties and the electronic structure of $MnWO_4$.

Recently, $MnWO_4$ has received much attention due to the finding that it exhibits ferroelectric (FE) polarization in the AF2 state,[5–7] because this state has a spiral-spin order[6,7] and hence has no inversion symmetry.[8–10] It was found that the spin spiral of the AF2 state propagates along the //*c*-chain direction as well as along the interlayer direction (i.e., the *a*

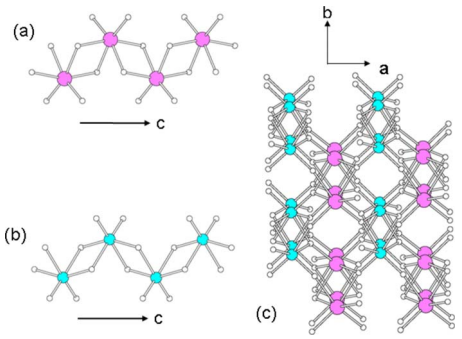

FIG. 1. (Color online) Perspective views of (a) a zigzag MnO_4 chain, (b) a zigzag WO_4 chain, and (c) the three-dimensional arrangement of the MnO_4 and WO_4 chains in $MnWO_4$. The Mn, W and O atoms are represented by large, medium and small circles, respectively.

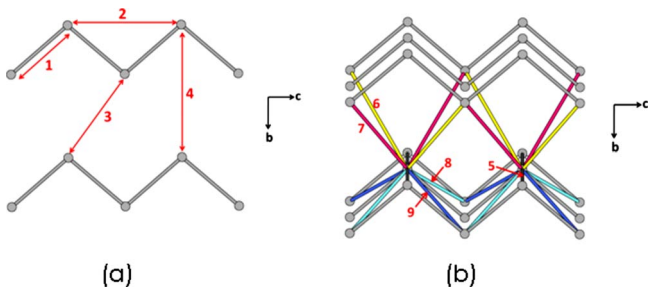

FIG. 2. (Color online) (a) Four spin exchange paths J_1–J_4 in $MnWO_4$ within each //*bc* layer of Mn^{2+} ions. (b) Five spin exchange paths J_5–J_9 between adjacent //*bc* layers of Mn^{2+} ions in $MnWO_4$. The numbers 1–9 refer to the spin exchange paths J_1–J_9, respectively.

TABLE I. Mn···Mn distances (in Å) associated with the spin exchange paths J_1-J_9 of $MnWO_4$ and the values of J_1-J_9 (in k_BK) determined by Ehrenberg *et al.* (Ref. 4) from their neutron scattering study and by the present GGA+U calculations.

	Mn···Mn	Ehrenberg *et al.*	GGA+U (U=4 eV)	GGA+U (U=6 eV)
J_1	3.283	−0.195	−2.343	−1.856
J_2	4.992	+0.414	−4.222	−2.691
J_3	4.398	−0.135	−0.174	−0.186
J_4	5.753	+0.021	−0.418	−0.209
J_5	4.823	−0.423	−2.714	−1.775
J_6	6.561	−1.273	−2.378	−1.334
J_7	6.492	+0.491	−0.638	−0.360
J_8	5.873	−0.509	−3.364	−2.146
J_9	5.795	+0.023	−1.601	−1.032

direction).[7] This implies that $MnWO_4$ has spin frustration in the exchange interactions within each //c chain and between the //c chains along the a direction, because noncollinear spin arrangements occur generally to reduce the extent of geometric spin frustration.[11–15] Indeed, $MnWO_4$ has been known to be a moderately spin frustrated system with the frustration parameter is $f=-\theta/T_N\approx 5$, where the Curie-Weiss temperature θ is approximately −75 K and the Néel temperature T_N is 13.5 K.[5,16] In the spin exchange values of Ehrenberg *et al.* (Table I),[4] the nearest-neighbor intrachain exchange J_1 is antiferromagnetic (AFM) while the next-nearest-neighbor intrachain exchange J_2 is FM. The latter means that the spin exchanges within each //c chain are not spin frustrated, which is inconsistent with the occurrence of spiral-spin within each //c chain.[7] The incommensurate (AF2 and AF3) and the commensurate (AF1) states have a common feature in their propagation vectors, i.e., the magnetic order along the b direction is AFM. The reason for this commensurate component is unclear, although one might speculate if it is a consequence of spin exchange interactions other than J_3 and J_4 because the latter two are quite weak according to Ehrenberg *et al.*[4] One drawback of spin exchange parameters deduced from experiment is that the physical data of a given magnetic system (e.g., magnetic susceptibility, inelastic neutron scattering and heat capacity data) are often fitted equally well by more than one set of exchange parameters, as found, for example, for $(VO)_2P_2O_7$,[17,18] $Na_3Cu_2SbO_6$ and $Na_2Cu_2TeO_6$,[19–23] and $Bi_4Cu_3V_2O_{14}$.[24–27] Ultimately, the correct set of exchange parameters should be consistent with the electronic structure of a magnetic system under consideration because it is the electronic structure that determines the magnetic energy spectrum.[28–31] In view of the fact that the magnetoelectric properties of $MnWO_4$ have attracted much attention in recent years, it is important to investigate the spin-exchange interactions and the FE polarization of $MnWO_4$ in terms of electronic structure calculations.

In the present work, we examine the magnetic and FE properties of $MnWO_4$ on the basis of first principles density functional theory (DFT) electronic structure calculations. We first evaluate the nine spin-exchange parameters of $MnWO_4$ by carrying out mapping analysis based on DFT calculations.[29] Then, we perform classical spin analysis[30] with the resulting spin exchange parameters to probe the incommensurate magnetic structure of $MnWO_4$. Finally, we evaluate the FE polarization of $MnWO_4$ by using the Berry phase method.[32,33]

II. COMPUTATIONAL DETAILS

Our calculations employed the Vienna *ab initio* simulation package,[34–36] the generalized gradient approximations (GGA) for the exchange and correlation corrections,[37] the plane-wave cutoff energy of 400 eV, 196 k points for the irreducible Brillouin zone, and the threshold of 10^{-6} eV for the self-consistent-field convergence of the total electronic energy. To properly describe the electron correlation of the Mn 3d states, the GGA plus on-site repulsion U(GGA+U) method[38] was employed with an effective U=4 and 6 eV on the Mn atom. The nine spin exchange parameters were evaluated by performing GGA+U calculations for a number of ordered spin states of $MnWO_4$ (see below). On the basis of the resulting spin exchange parameters, we examined the magnetic structure of $MnWO_4$ by performing classical spin analysis as described elsewhere.[30] For the ferroelectricity driven by a magnetic order, it is essential to take into consideration spin-orbit coupling (SOC) effects in electronic structure calculations.[13–15] Thus, to estimate the FE polarization of $MnWO_4$ in the AF2 state, we performed GGA+U +SOC calculations for a model spiral-spin state of $MnWO_4$ (see below), which is designed to simulate the AF2 state of $MnWO_4$. Then, the FE polarization was calculated by using the Berry phase method.[32,33]

III. SPIN EXCHANGE PARAMETERS

In the magnetic state AF1 the $\uparrow\uparrow\downarrow\downarrow$ spin order occurs along the c and the a directions, and the $\uparrow\downarrow\uparrow\downarrow$ spin arrangement along the b direction. In addition, the phase of the $\uparrow\uparrow\downarrow\downarrow$ arrangement along the a direction is shifted such that four different $\uparrow\uparrow\downarrow\downarrow$ arrangements occur (i.e., $\uparrow\downarrow\downarrow\uparrow$, $\downarrow\downarrow\uparrow\uparrow$, $\downarrow\uparrow\uparrow\downarrow$, $\uparrow\uparrow\downarrow\downarrow$). Consequently, the propagation vector of the AF1 state becomes (−0.25, 0.5, 0.5). In general, the $\uparrow\uparrow\downarrow\downarrow$ arrangement along a certain direction occurs when there is geometric spin frustration, as found for the CuO_2 ribbon chains of $LiCuVO_4$ and $LiCu_2O_2$.[13] The propagation vector of the incommensurate states AF2 and AF3, (−0.214, 0.5, 0.457), is slightly different from that of the AF1 state. To gain insight into the occurrence of the ordered magnetic states AF1 and AF2 of $MnWO_4$, we evaluate its spin-exchange parameters J_1-J_9 and discuss their trends.

A. Mapping analysis

To evaluate J_1-J_9, we examine the 10 ordered spin states defined in Figs. 3–5. The relative energies of these states determined from our GGA+U calculations are summarized in Table II. To extract the values of the spin-exchange parameters J_1-J_9, we express the total spin exchange interac-

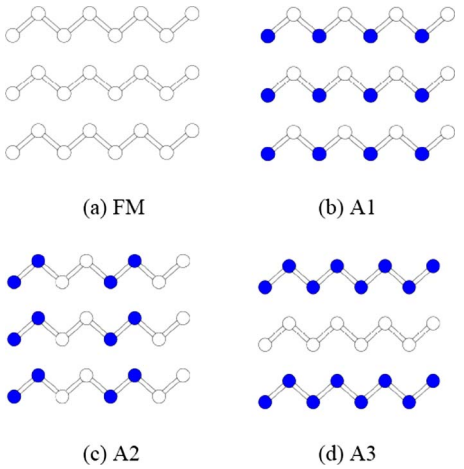

FIG. 3. (Color online) Ordered spin arrangements in each $//bc$ layer of Mn^{2+} ions in the FM, A1, A2, and A3 states of $MnWO_4$. The up-spin and down-spin Mn^{2+} sites are represented by filled and unfilled circles, respectively.

tion energies of the 10 ordered spin states in terms of the spin Hamiltonian,

$$\hat{H} = -\sum_{i<J} J_{ij}\hat{S}_i \cdot \hat{S}_j, \tag{1}$$

where $J_{ij}(=J_1-J_9)$ is the spin exchange parameter for the spin exchange interaction between the spin sites i and j, while $\hat{S}_i$ and $\hat{S}_j$ are the spin angular momentum operators at the spin sites i and j, respectively. Then, by applying the energy expressions obtained for spin dimers with N unpaired spins per spin site (in the present case, $N=5$),[39,40] the total spin exchange energies of the 10 ordered spin states (per two formula units) are written as

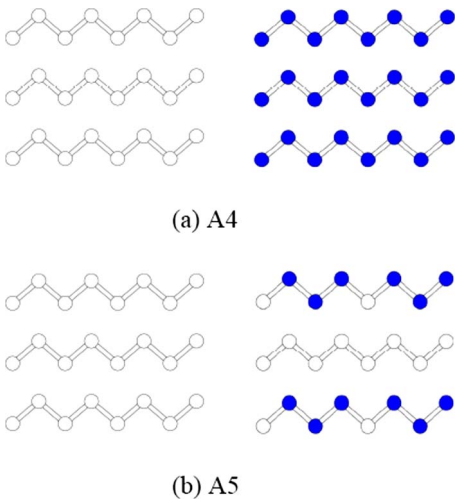

FIG. 4. (Color online) Ordered spin arrangements in two successive $//bc$ layers of Mn^{2+} ions in the A4 and A5 states of $MnWO_4$. The up-spin and down-spin Mn^{2+} sites are represented by filled and unfilled circles, respectively.

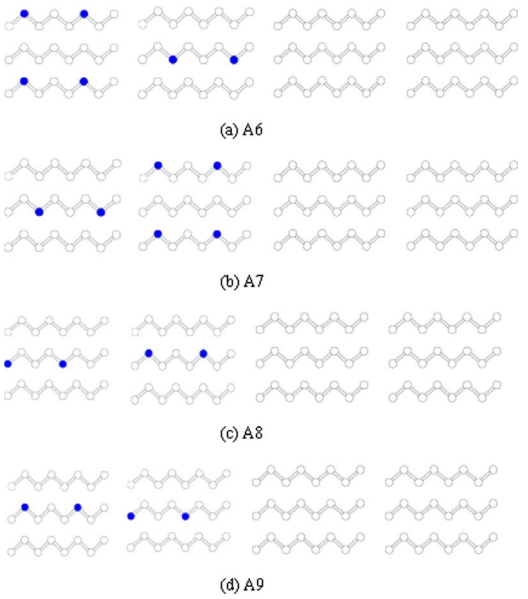

FIG. 5. (Color online) Ordered spin arrangements in four successive $//bc$ layers of Mn^{2+} ions in the A6, A7, A8, and A9 states of $MnWO_4$. The up-spin and down-spin Mn^{2+} sites are represented by filled and unfilled circles, respectively.

$$E_{\mathrm{FM}} = (-2J_1 - 2J_2 - 2J_3 - 2J_4 - 2J_5 - 2J_6 - 2J_7 - 2J_8 - 2J_9) \times (N^2/4)$$

$$E_{\mathrm{AF1}} = (+2J_1 - 2J_2 + 2J_3 - 2J_4 - 2J_5 + 2J_6 + 2J_7 + 2J_8 + 2J_9) \times (N^2/4)$$

$$E_{\mathrm{AF2}} = (+2J_2 - 2J_4 - 2J_5)(N^2/4)$$

$$E_{\mathrm{AF3}} = (-2J_1 - 2J_2 + 2J_3 + 2J_4 - 2J_5 + 2J_6 + 2J_7 - 2J_8 - 2J_9) \times (N^2/4)$$

$$E_{\mathrm{AF4}} = (-2J_1 - 2J_2 - 2J_3 - 2J_4 + 2J_5 + 2J_6 + 2J_7 + 2J_8 + 2J_9) \times (N^2/4)$$

TABLE II. Relative energies (in meV per two formula units) of the ordered spin states of $MnWO_4$ determined by the present GGA+U calculations.

	U=4 eV	U=6 eV
FM	0.00	0.00
A1	−22.62	−14.88
A2	−20.42	−13.24
A3	−7.75	−4.49
A4	−23.04	−14.32
A5	−10.88	−6.91
A6	−4.72	−3.07
A7	−4.49	−2.94
A8	−4.35	−2.83
A9	−4.59	−2.98

$$E_{AF5} = (-3J_1 - 3J_2 - J_3 - J_4 - J_5 - J_6 - J_7 - J_8 - J_9)(N^2/8)$$

$$E_{AF6} = (-3J_1 - 3J_2 - 3J_3 - 3J_4 - 3J_5 - 3.5J_6 - 3J_7 - 3J_8 - 3J_9)(N^2/8)$$

$$E_{AF7} = (-3J_1 - 3J_2 - 3J_3 - 3J_4 - 3J_5 - 3J_6 - 3J_7 - 3.5J_8 - 3J_9)(N^2/8)$$

$$E_{AF8} = (-3J_1 - 3J_2 - 3J_3 - 3J_4 - 3J_5 - 3.5J_6 - 3.5J_7 - 3J_8 - 3J_9)(N^2/8)$$

$$E_{AF9} = (-3J_1 - 3J_2 - 3J_3 - 3J_4 - 3J_5 - 3J_6 - 3J_7 - 3J_8 - 3.5J_9)(N^2/8). \quad (2)$$

Thus, by mapping the relative energies of the ten-ordered spin states determined by the GGA+U calculations onto the corresponding relative energies determined from the above spin-exchange energies, we obtain the values of J_1-J_9 summarized in Table I.

B. Trends in the spin exchange interactions

Let us first comment on the values of J_1-J_9 calculated in the previous section. In the mean field theory,[41] which is valid in the high-temperature paramagnetic limit, the Curie-Weiss temperature θ is related to the spin exchange parameters of $MnWO_4$ as follows:

$$\theta = \frac{S(S+1)}{3k_B}\sum_i z_i J_i, \quad (3)$$

where the summation runs over all nearest neighbors of a given spin site, z_i is the number of nearest neighbors connected by the spin exchange parameter J_i, and S is the spin quantum number of each spin site Mn^{2+} (i.e., $S=5/2$ in the present case). Thus, according to the spin exchange paths defined in Fig. 2, θ is expressed as

$$\theta = \frac{20(J_1 + J_2 + J_3 + J_4 + J_5 + J_6 + J_7 + J_8 + J_9)}{k_B}. \quad (4)$$

From the J_i values from the GGA+U calculations (Table I), the Curie-Weiss temperature is found to be $\theta_{cal}=-357$ and -232 K for $U=4$ and 6 eV, respectively. The experimental Curie-Weiss temperature is $\theta_{exp}\approx -75$ K, so that θ_{cal} is greater than θ_{exp} by a factor of approximately 3–5. The latter means that the calculated J_i values are overestimated by a factor of approximately 3–5, which is consistent with the finding that DFT electronic structure calculations generally overestimate the magnitude of spin exchange interactions by a factor of approximately 4.[39,42–44] In terms of the J_i values of Ehrenberg *et al.*[4] (Table I) the Curie-Weiss temperature is calculated to be -32 K, so that their J_i values are underestimated by a factor of approximately 2.5 as far as the Curie-Weiss temperature is concerned.

Our calculations (Table I) show that both J_1 and J_2 are AFM, and $J_2/J_1 \geqslant 0.25$, so that geometric spin frustration exists within each $//c$ chain. This finding accounts for the occurrence, in each $//c$ chain, of the spiral-spin order in the AF2 state and the $\uparrow\uparrow\downarrow\downarrow$ spin order in the AF1 state. To see if there exists spin frustration along the a-direction, we consider four commensurate spin arrangements of $MnWO_4$ generated by using the $//c$ chains with $\uparrow\uparrow\downarrow\downarrow$ spin order as the building units (Figure 6). In the AF1 state [Fig. 6(a)], the $//c$-chains have a $\uparrow\downarrow\uparrow\downarrow$ order (i.e., an AFM coupling) along the b direction and a $\uparrow\uparrow\downarrow\downarrow$ spin order along the a direction. The AF4 state [Fig. 6(b)] differs from the AF1 state, only in that the $//c$ chains have a $\uparrow\downarrow\uparrow\downarrow$ order along the a direction. The AF5 [Fig. 6(c)] and AF6 [Fig. 6(d)] states differ from the AF1 and AF4 states only in that the $//c$ chains have a $\uparrow\uparrow\uparrow\uparrow$ order (i.e., an FM coupling) along the b direction, respectively. Per spin site, these four commensurate spin arrangements give rise to the interchain spin exchange energies listed in Table III. The exchange parameters J_1-J_9 of Ehrenberg *et al.* as well as those obtained from our GGA+U calculations predict that the AF1 state is the most stable state of the four. The J_1-J_9 values from the GGA+U calculations show that the $//c$ chains with $\uparrow\uparrow\downarrow\downarrow$ spin order prefer to have a $\uparrow\downarrow\uparrow\downarrow$ order rather than a $\uparrow\uparrow\uparrow\uparrow$ order along the b direction, in agreement with experiment. Furthermore, the J_1-J_9 values from the GGA+U calculations predict that the AF4 state (i.e., a $\uparrow\downarrow\uparrow\downarrow$ order along the a direction) is close in energy to the AF1 state (i.e., a $\uparrow\uparrow\downarrow\downarrow$ order along the a direction). In other words, along the a direction, the interaction between the $//c$ chains with the $\uparrow\uparrow\downarrow\downarrow$ spin order is effectively frustrated because the spin order can be either $\uparrow\uparrow\downarrow\downarrow$ or $\uparrow\downarrow\uparrow\downarrow$, the extent of which may be reduced by an incommensurate spiral-spin order along the a direction. This topic will be discussed further in the next section.

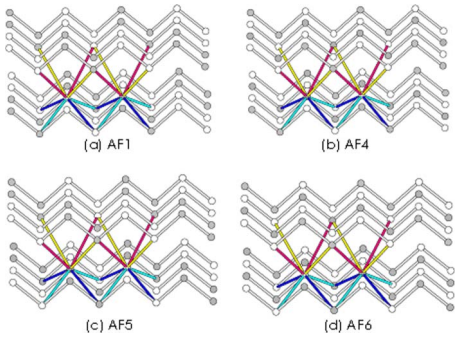

FIG. 6. (Color online) Spin arrangements of the (a) AF1, (b) AF4, (c) AF5, and (d) AF4 states of $MnWO_4$, which are generated in terms of the $//c$ chains with the $\uparrow\uparrow\downarrow\downarrow$ spin order.

IV. CLASSICAL SPIN ANALYSIS

To examine the occurrence of the incommensurate magnetic structure (i.e., the AF2 and AF3 states) in $MnWO_4$, we calculate the total spin exchange energy of $MnWO_4$ by using the Freiser method.[30,45] This approach assumes that spins adopt all possible directions in space (i.e., the classical spin approximation), and the spin-exchange interactions are isotropic (i.e., a Heisenberg description). These assumptions are appropriate for $MnWO_4$, because the local magnetic anisotropy of the high spin Mn^{2+} ($S=5/2$, $L=0$) ions is very

TABLE III. Four arrangements of the $//c$ chains with $\uparrow\uparrow\downarrow\downarrow$ spin order and their interchain spin exchange energies, E, per spin site.

	$//b$	$//a$	E (per Mn)	E (k_BK per Mn)[a]		
				Case A	Case B	Case C
AF1	$\uparrow\downarrow\uparrow\downarrow$	$\uparrow\uparrow\downarrow\downarrow$	$+J_6-J_7+J_8-J_9+J_4$	−2.75	−3.92	−2.30
AF4	$\uparrow\downarrow\uparrow\downarrow$	$\uparrow\downarrow\uparrow\downarrow$	$+J_5+J_4$	−0.40	−3.13	−1.98
AF5	$\uparrow\uparrow\uparrow\uparrow$	$\uparrow\uparrow\downarrow\downarrow$	$-J_6+J_7+J_8-J_9-J_4$	+1.21	+0.40	+0.07
AF6	$\uparrow\uparrow\uparrow\uparrow$	$\uparrow\downarrow\uparrow\downarrow$	$+J_5-J_4$	−0.44	−2.30	−1.57

[a]Case A: Calculated from the J_1-J_9 by Ehrenberg *et al.* Case B: Calculated from the J_1-J_9 of the present GGA+U calculations with $U=4$ eV. Case C: Calculated from the J_1-J_9 of the present GGA+U calculations with $U=6$ eV.

small. Indeed, $MnWO_4$ is well described as a Heisenberg antiferromagnet, as shown by the very small anisotropy of the paramagnetic susceptibility.[5] This also means that the complex low-temperature magnetic properties of $MnWO_4$ do not arise from a competition between the local anisotropy and the spin-exchange interactions, but from the frustration of the spin-exchange interactions.

In a long-range ordered magnetic state of a magnetic system, the spin sites $\mu(=1,2,\ldots,m)$ of its unit cell located at the coordinate origin (i.e., the lattice vector $\mathbf{R}=0$) have the spin moments $\boldsymbol{\sigma}_\mu^0$. For a magnetic solid with repeat vectors **a**, **b**, and **c**, the ordered spin arrangement is described by the spin functions $\boldsymbol{\sigma}_\mu(\mathbf{k})$,

$$\boldsymbol{\sigma}_\mu(\mathbf{k}) = \frac{1}{\sqrt{M}}\sum_{\mathbf{R}} \boldsymbol{\sigma}_\mu^0 \exp(i\mathbf{k}\cdot\mathbf{R}), \tag{5}$$

where M is the number of unit cells in the magnetic solid, **k** is the wave vector, and **R** is the direct lattice vector.[46] The ordered magnetic state $\psi_i(\mathbf{k})$ $(i=1-m)$ is then expressed as a linear combination of the spin functions $\boldsymbol{\sigma}_\mu(\mathbf{k})$,

$$\psi_i(\mathbf{k}) = C_{1i}(\mathbf{k})\boldsymbol{\sigma}_1(\mathbf{k}) + C_{2i}(\mathbf{k})\boldsymbol{\sigma}_2(\mathbf{k}) + \cdots + C_{mi}(\mathbf{k})\boldsymbol{\sigma}_m(\mathbf{k}). \tag{6}$$

To determine the energy $E_i(\mathbf{k})$ of the state $\psi_i(\mathbf{k})$ and the coefficients $C_{\mu i}(\mathbf{k})$ $(\mu=1-m)$, one needs to evaluate the spin exchange interaction energies $\xi_{\mu\nu}(\mathbf{k})$ between every two spin functions $\boldsymbol{\sigma}_\mu(\mathbf{k})$ and $\boldsymbol{\sigma}_\nu(\mathbf{k})$,

$$\xi_{\mu\nu}(\mathbf{k}) = -\sum_{\mathbf{R}} \mathbf{J}_{\mu\nu}(\mathbf{R})\exp(i\mathbf{k}\cdot\mathbf{R}), \tag{7}$$

where $J_{\mu\nu}(\mathbf{R})=J_1$, J_2, J_3, J_4, J_5, J_6, J_7, J_8, or J_9. The resulting interaction matrix $\boldsymbol{\Xi}(\mathbf{k})$ is given by

$$\boldsymbol{\Xi}(\mathbf{k}) = \begin{pmatrix} \xi_{11}(\mathbf{k}) & \xi_{12}(\mathbf{k}) & \cdots & \xi_{1m}(\mathbf{k}) \\ \xi_{21}(\mathbf{k}) & \xi_{22}(\mathbf{k}) & \cdots & \xi_{2m}(\mathbf{k}) \\ \cdots & \cdots & \cdots & \cdots \\ \xi_{m1}(\mathbf{k}) & \xi_{m2}(\mathbf{k}) & \cdots & \xi_{mm}(\mathbf{k}) \end{pmatrix}. \tag{8}$$

We obtain $E_i(\mathbf{k})$ of the state $\psi_i(\mathbf{k})$ by diagonalizing this matrix. This method predicts the superstructure of a magnetic system by finding the wave vector at which its global energy minimum occurs.[30,45]

There are two Mn^{2+} ion sites in a crystallographic unit cell of $MnWO_4$ [Table IV(a)], so that $m=2$ in Eq. (8). The spin exchanges J_1-J_9 occur for various pairs of spin sites (μ,ν) within a unit cell located at [0, 0, 0] as well as between adjacent unit cells [0, 0, 0] and $[n,k,l]$ $(n,k,l=-1,0,+1)$, as summarized in Table IV(b). Consequently, we obtain the following matrix elements $\xi_{\mu\nu}(\mathbf{k})$ $(\mu,\nu=1,2)$,

TABLE IV. (a) Fractional coordinates of the spin sites in $MnWO_4$ (b) Pairs (μ,ν) of the spin sites $(\mu,\nu=1,2)$ leading to the spin exchanges J_1-J_9 in $MnWO_4$ within a unit cell at [0, 0, 0] as well as between unit cells [0, 0, 0] and $[n,k,l]$

(a) Spin site	Mn	x	y	z
1	Mn(1)	0.5	0.6853	0.25
2	Mn(2)	0.5	0.3147	0.75

(b) Path	Within	Between	$[n,k,l]$
J_1	(1,2)	(1,2)	[0,0,−1]
	(2,1)	(2,1)	[0,0,1]
J_2		(1,1)	[0,0,−1] and [0,0,1]
		(2,2)	[0,0,−1] and [0,0,1]
J_3		(1,2)	[0,1,0] and [0,1,−1]
		(2,1)	[0,−1,0] and [0,−1,1]
J_4		(1,1)	[0,1,0] and [0,−1,0]
		(2,2)	[0,1,0] and [0,−1,0]
J_5		(1,1)	[1,0,0] and [−1,0,0]
		(2,2)	[1,0,0] and [−1,0,0]
J_6		(1,2)	[1,1,−1] and [−1,1,0]
		(2,1)	[−1,−1,1] and [1,−1,0]
J_7		(1,2)	[−1,1−1] and [1,1,0]
		(2,1)	[1,−1,1] and [−1,−1,0]
J_8		(1,2)	[1,0,−1] and [−1,0,0]
		(2,1)	[−1,0,1] and [1,0,0]
J_9		(1,2)	[1,0,0] and [−1,0,−1]
		(2,1)	[−1,0,0] and [1,0,1

$$\xi_{11}(\mathbf{k}) = \xi_{22}(\mathbf{k}) = -J_2[\exp(-i2\pi x_c) + \exp(+i2\pi x_c)] - J_4[\exp(-i2\pi x_b) + \exp(+i2\pi x_b)] - J_5[\exp(-i2\pi x_a) + \exp(+i2\pi x_a)]$$

$$\xi_{12}(\mathbf{k}) = \xi_{21}(\mathbf{k})^* = -J_1\{1 + \exp[i2\pi(-x_c)]\} - J_3\{\exp[i2\pi(+x_b)] + \exp[i2\pi(+x_b - x_c)]\} - J_6\{\exp[i2\pi(+x_a + x_b - x_c)] + \exp[i2\pi(-x_a + x_b)]\} - J_7\{\exp[i2\pi(-x_a + x_b - x_c)] + \exp[i2\pi(+x_a + x_b)]\} - J_8\{\exp[i2\pi(+x_a - x_c)] + \exp[i2\pi(-x_a)]\} - J_9\{\exp[i2\pi(+x_a)] + \exp[i2\pi(-x_a - x_c)]\} \quad (9)$$

where x_a, x_b, and x_c are dimensionless numbers.[46]

Thus, at any given wave vector $\mathbf{k}$, one can determine the numerical values of $\xi_{\mu\nu}(\mathbf{k})$ $(\mu,\nu=1,2)$ by using the J_1-J_9 values listed in Table I and hence diagonalize the $\Xi(\mathbf{k})$ matrix to obtain $E_i(\mathbf{k})$ $(i=1,2)$. Then, the propagation vector $\mathbf{q}$ of the incommensurate magnetic state is determined as the $\mathbf{k}$ value at which the lower energy $E_1(\mathbf{k})$ has the minimum. Our calculations show that $\mathbf{q}=(-0.29,0.5,0.44)$ from the J_1-J_9 values of Ehrenberg *et al.*, and (−0.35, 0.5, 0.49) and (−0.36, 0.5, 0.48) from the calculated J_1-J_9 values with $U=4$ and 6 eV, respectively. These results are in qualitative agreement with the appearance of the incommensurate AF2 state with $\mathbf{q}=(-0.214,0.5,0.457)$. From this finding and our discussion in the previous section (Fig. 6), it is clear that the AFM coupling along the b direction both in the incommensurate state AF2 and in the commensurate state AF1 arises to lower the energy associated with the spin-exchange interactions other than the weak interchain exchanges J_3 and J_4.

The observation of the collinear commensurate state AF1 as the magnetic ground state below 8 K is due most likely to a weak local magnetic anisotropy of Mn^{2+}, which is not included in the Heisenberg model. Since the entropy is greater in the spiral-spin incommensurate state AF2 than in the collinear commensurate AF1 state, the AF2 state would be energetically favored over the AF1 state at temperature higher than 8 K. It is interesting to note that doping the Mn^{2+} sites of $MnWO_4$ with a small amount of Fe^{2+} (d^6, $S=2$) ions stabilizes the AF1 state,[47] which is due to the large local magnetic anisotropy of the high-spin Fe^{2+} ions.

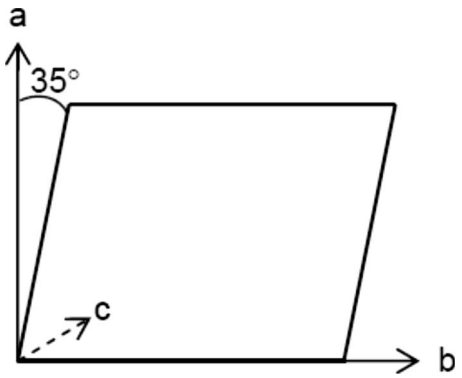

FIG. 7. Plane of spin spiral found in $MnWO_4$.

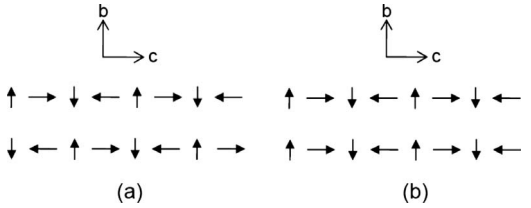

FIG. 8. Two arrangements of the $//c$ chains of Mn^{2+} ions with spiral-spin order along the b direction: (a) AFM and (b) FM. The zigzag chains are represented as straight chains to emphasize the spin spiral order.

V. FERROELECTRIC POLARIZATION

In this section, we examine the FE polarization of the spiral-spin state AF2 of $MnWO_4$. The spin-spiral plane is perpendicular to the ac-plane and is tilted away from the a-axis by 35° (Fig. 7). The incommensurate propagation vector of the AF2 state is (−0.214, 0.5, 0.457), the closest commensurate approximation of which is (−0.25, 0.5, 0.5). The latter requires the use of the supercell ($4a$, $2b$, $2c$) for our GGA+U+SOC calculations of FE polarization. Fig. 8 shows the AFM and FM arrangements, along the b direction, of the $//c$ chains with spiral-spin order. In both the AFM and the FM arrangements, each $//c$ chain has the same chirality of spin spiral, and hence leads to a same sign of FE polarization. In addition, the interchain exchange interactions J_3 and

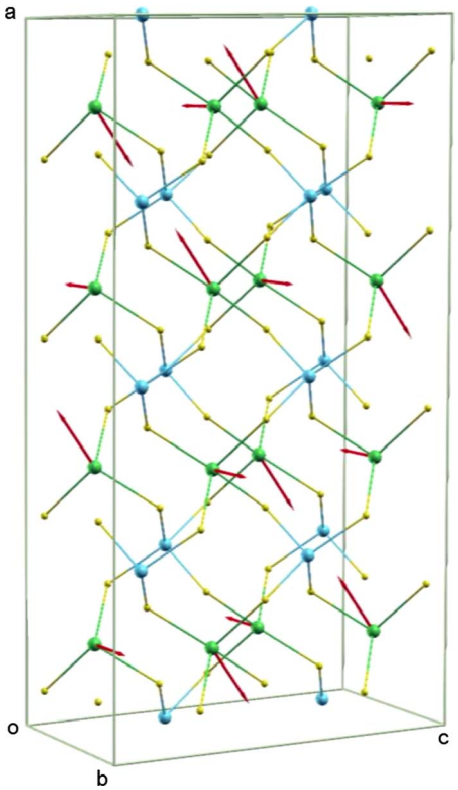

FIG. 9. (Color online) Perspective view of the commensurate spiral-spin arrangement of $MnWO_4$ within a ($4a$, b, $2c$) supercell, which was employed for the GGA+U+SOC calculation of FE polarization. The plane of the spin spiral is defined as in Fig. 7, so that the spins spiral along the a and c directions.

J_4 are very weak, as already mentioned. Thus, for the purpose of FE polarization, we assume the FM ordering of the $//c$ chains along the b direction and, hence, employ the supercell ($4a$, b, $2c$) for our calculations. In making the spiral-spin arrangement with the ($4a$, b, $2c$) supercell, we employed the plane of the spin spiral defined in Fig. 7 so that the spins spiral along the a and c directions. In our GGA+U+SOC calculations (with U=6 eV) for the electronic structure of this model spiral-spin state, the atom positions of the ($4a$, b, $2c$) supercell were not relaxed (Fig. 9). Our subsequent Berry phase calculations show that the FE polarization is along the positive b direction with P_b=17.2 μC/m^2. Experimentally, P_b is found to be smaller than ~50 μC/m^2.[5]

It is of interest to examine the calculated FE polarization from the viewpoint of the Katsura-Nagaosa-Balatsky (KNB) model,[48] which predicts that the FE polarization $\vec{P}$ of a spiral-spin chain with spins $\vec{S}_i$ and $\vec{S}_j$ at the adjacent spin sites connected by the vector $\vec{e}_{ij}$ is given by

$$\vec{P} \propto \vec{e}_{ij} \times (\vec{S}_i \times \vec{S}_j), \tag{10}$$

according to which FE polarization arises only from spin-spiral chains of cycloidal type (i.e., those chains whose spin-spiral planes contain the chains). In the ($4a$, b, $2c$) superstructure with the (−0.25, 0, 0.5) spiral-spin order, the spiral-spin propagation along the a direction has a cycloidal component when the spins are projected on the ab plane [Fig. 10(a)], while that along the c direction has a cycloidal component when the spins are projected on the bc plane (Fig. 10(b)). It is reasonable to assume that the sign of the coefficient in Eq. (10) for the ab plane is the same as that for the bc plane. Then, the cycloidal component in the ab plane gives a positive FE polarization along the b direction [Fig. 10(a)], whereas that in the bc plane gives a negative FE polarization along the b direction [Fig. 10(b)]. Since the angle between the ab and the spin-spiral planes is 35°, the FE polarization arising from the ab plane cycloidal component is greater than that from the bc plane cycloidal component. As a consequence, the net FE polarization is along the positive b direction, as found from our GGA+U calculations.

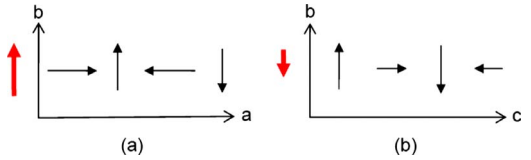

FIG. 10. (Color online) Cycloidal components of the spiral-spin state with the ($4a$, b, $2c$) superstructure used to simulate the spiral-spin ordered state AF2. (a) The projection view of the spiral-spin propagation along the a direction on the ab plane. (b) that along the c direction on the bc plane, where the zigzag chain was represented as a straight chain to emphasize the spin spiral order. The polarization direction is represented by red arrows.

VI. CONCLUDING REMARKS

The spin exchange interactions of $MnWO_4$ extracted from the present GGA+U calculations reveal that the spin exchange interactions are frustrated within each $//c$ chain of Mn^{2+} ions and between such $//c$ chains along the a direction. This finding is in agreement with the experimental observation that a spiral-spin propagates along the c and the a directions in the incommensurate state AF2, and a $\uparrow\uparrow\downarrow\downarrow$ spin arrangement occurs along the c and a directions in the collinear magnetic state AF1. The classical spin analysis with the extracted spin-exchange parameters leads to an incommensurate state with propagation vector in qualitative agreement with that found for the AF2 state. The AFM coupling between the $//c$ chains along the b direction does not result from the weak interchain exchanges J_3 and J_4 but from the combined effect of other strong spin exchange interactions. The Berry phase calculations for a model ($4a$, b, $2c$) superstructure with spiral-spin order show FE polarization along the b direction, in agreement with experiment.

ACKNOWLEDGMENTS

The research was supported by the Office of Basic Energy Sciences, Division of Materials Sciences, U.S. Department of Energy, under Grant No. DE-FG02-86ER45259, and by the NERSC Center (under Contract No. DE-AC02-05CH11231) and the HPC Center of the NCSU campus.

[1] H. Weitzel, Z. Kristallogr. **144**, 238 (1976).
[2] J. Macavei and H. Schulz, Z. Kristallogr. **207**, 193 (1993).
[3] G. Lautenschläger, H. Weitzel, T. Vogt, R. Hock, A. Böhm, M. Bonnet, and H. Fuess, Phys. Rev. B **48**, 6087 (1993).
[4] H. Ehrenberg, H. Weitzel, H. Fuess, and B. Hennion, J. Phys.: Condens. Matter **11**, 2649 (1999).
[5] A. H. Arkenbout, T. T. M. Palstra, T. Siegrist, and T. Kimura, Phys. Rev. B **74**, 184431 (2006).
[6] O. Heyer, N. Hollmann, I. Klassen, S. Jodlauk, L. Bohatý, P. Becker, J. A. Mydosh, T. Lorenz, and D. Khomskii, J. Phys.: Condens. Matter **18**, L471 (2006).
[7] K. Taniguchi, N. Abe, T. Takenobu, Y. Iwasa, and T. Arima, Phys. Rev. Lett. **97**, 097203 (2006).
[8] M. Fiebig, J. Phys. D **38**, R123 (2005).
[9] Y. Tokura, Science **312**, 1481 (2006).
[10] S.-W. Cheong and M. Mostvoy, Nature Mater. **6**, 13 (2007).
[11] J. E. Greedan, J. Mater. Chem. **11**, 37 (2001).
[12] D. Dai and M.-H. Whangbo, J. Chem. Phys. **121**, 672 (2004).
[13] H. J. Xiang and M.-H. Whangbo, Phys. Rev. Lett. **99**, 257203 (2007).
[14] H. J. Xiang, C. Lee, and M.-H. Whangbo, Phys. Rev. B **76**, 220411(R) (2007).
[15] H. J. Xiang, S.-H. Wei, M.-H. Whangbo, and J. L. F. Da Silva, Phys. Rev. Lett. **101**, 037209 (2008).
[16] H. Dachs, Solid State Commun. **7**, 1015 (1969).
[17] A. W. Garrett, S. E. Nagler, D. A. Tennant, B. C. Sales, and T.

Barnes, Phys. Rev. Lett. **79**, 745 (1997).
[18] H.-J. Koo, M.-H. Whangbo, P. D. VerNooy, C. C. Torardi, and W. J. Marshall, Inorg. Chem. **41**, 4664 (2002).
[19] J. Xu, A. Assoud, N. Soheilnia, S. Derakhshan, H. L. Cuthbert, J. E. Greedan, M.-H. Whangbo, and H. Kleinke, Inorg. Chem. **44**, 5042 (2005).
[20] Y. Miura, R. Hirai, Y. Kobayashi, and M. Sato, J. Phys. Soc. Jpn. **75**, 084707 (2006).
[21] S. Derakhshan, H. L. Cuthbert, J. E. Greedan, B. Rahaman, and T. Saha-Dasgupta, Phys. Rev. B **76**, 104403 (2007).
[22] H.-J. Koo and M.-H. Whangbo, Inorg. Chem. **47**, 128 (2008).
[23] Y. Miura, Y. Yasui, T. Moyoshi, M. Sato, and K. Kakurai, J. Phys. Soc. Jpn. **77**, 104709 (2008).
[24] H. Sakurai, K. Yoshimura, K. Kosuge, N. Tsujii, H. Abe, H. Kitazawa, G. Kido, H. Michor, and G. Hilscher, J. Phys. Soc. Jpn. **71**, 1161 (2002).
[25] S. Okubo, T. Hirano, Y. Inagaki, H. Ohta, H. Sakurai, H. Yoshimura, and K. Kosuge, Physica B **346-347**, 65 (2004).
[26] K. Okamoto, T. Tonegawa, and M. Kaburagi, J. Phys.: Condens. Matter **15**, 5979 (2003).
[27] H.-J. Koo and M.-H. Whangbo, Inorg. Chem. **47**, 4779 (2008).
[28] F. Illas, I. P. R. Moreira, C. de Graaf, and D. Varone, Theor. Chem. Acc. **104**, 265 (2000).
[29] M.-H. Whangbo, H.-J. Koo, and D. Dai, J. Solid State Chem. **176**, 417 (2003).
[30] M.-H. Whangbo, D. Dai, and H.-J. Koo, Solid State Sci. **7**, 827 (2005).
[31] D. Dai, H. J. Xiang, and M.-H. Whangbo, J. Comput. Chem. **29**, 2187 (2008).
[32] R. D. King-Smith and D. Vanderbilt, Phys. Rev. B **47**, 1651 (1993).
[33] R. Resta, Rev. Mod. Phys. **66**, 899 (1994).
[34] G. Kresse and J. Hafner, Phys. Rev. B **47**, 558 (1993).
[35] G. Kresse and J. Furthmüller, Comput. Mater. Sci. **6**, 15 (1996).
[36] G. Kresse and J. Furthmüller, Phys. Rev. B **54**, 11169 (1996).
[37] J. P. Perdew, K. Burke, and M. Ernzerhof, Phys. Rev. Lett. **77**, 3865 (1996).
[38] S. L. Dudarev, G. A. Botton, S. Y. Savrasov, C. J. Humphreys, and A. P. Sutton, Phys. Rev. B **57**, 1505 (1998).
[39] D. Dai and M.-H. Whangbo, J. Chem. Phys. **114**, 2887 (2001).
[40] D. Dai and M.-H. Whangbo, J. Chem. Phys. **118**, 29 (2003).
[41] J. S. Smart, *Effective Field Theory of Magnetism* (Saunders, Philadelphia, 1966).
[42] D. Dai, H.-J. Koo, and M.-H. Whangbo, J. Solid State Chem. **175**, 341 (2003).
[43] D. Dai, M.-H. Whangbo, M.-H. Koo, X. Rocquefelte, S. Jobic, and A. Villesuzanne, Inorg. Chem. **44**, 2407 (2005).
[44] R. Grau-Crespo, N. H. de Leeuw, and C. R. Catlow, J. Mater. Chem. **13**, 2848 (2003).
[45] M. J. Freiser, Phys. Rev. **123**, 2003 (1961).
[46] Given the lattice vector written as $\mathbf{R}=n_a\mathbf{a}+n_b\mathbf{b}+n_c\mathbf{c}$, where n_a, n_b, and n_c are integers, and the wave vector $\mathbf{k}$ written as $\mathbf{k}=x_a\mathbf{a}^*+x_b\mathbf{b}^*+x_c\mathbf{c}^*$, where $\mathbf{a}^*$, $\mathbf{b}^*$, and $\mathbf{c}^*$ are the reciprocal vectors, and x_a, x_b, and x_c are dimensionless numbers, the $\exp(i\mathbf{k}\cdot\mathbf{R})$ term becomes $\exp[i2\pi(x_an_a+x_bn_b+x_cn_c)]$.
[47] F. Ye, Y. Ren, J. A. Fernandez-Baca, H. A. Mook, J. W. Lynn, R. P. Chaudhury, Y. Q. Wang, B. Lorenz, and C. W. Chu, Phys. Rev. B **78**, 193101 (2008).
[48] H. Katsura, N. Nagaosa, and A. V. Balatsky, Phys. Rev. Lett. **95**, 057205 (2005).